Calculation of transport profiles in modulation experiments with source without transport codes

D.F. Escande[1], F. Sattin[2], Y. Camenen[1], A.T. Salmi[3], T. Tala[3] and JET EFDA Contributors[*]

[1] Laboratoire PIIM, UMR 7345 CNRS-Aix Marseille Université, France

[2] Consorzio RFX, Associazione EURATOM-ENEA sulla fusione, Padova, Italy

[3]Association Euratom-Tekes, VTT, P.O. Box 1000, FI-02044 VTT, Finland

E-mail contact of main author: dominique.escande@univ-amu.fr

Abstract. Transport codes provide a classical way to infer the profile of transport coefficients in fusion plasmas with sources: assuming given functionals for the transport coefficient profiles, the free parameters are iteratively adjusted to best reproduce the measurements. This work discusses a technique for the case of modulated experiments with sources, the matrix approach (MA), which avoids any *a priori* constraint of the profiles, and computes them by simply inverting pointwise a 2D matrix.

1. Introduction

This paper deals with the analysis of transport in modulation experiments with the standard convective-diffusive paradigm, i.e. in terms of a diffusion coefficient $D(r)$ and of a pinch velocity $V(r)$. Transport codes provide a classical way to infer the profile of the coefficients in fusion plasmas with sources: $D(r)$ and $V(r)$ are guessed in terms of simple functionals, whose free parameters are iteratively adjusted until the best match between the experiment and the simulation by the code is reached. Unfortunately this procedure does not easily provide information of the uncertainty in the transport profile reconstruction. This issue is not trivial, since inferring $D(r)$ and $V(r)$ from measurements is an inverse problem. As such it may be ill conditioned—that is, the outcome may depend sensitively from any small change in the input. This paper discusses and provides some applications of the matrix approach (MA) to modulation experiments, which avoids any *a priori* constraint of the profiles, and computes $D(r)$ and $V(r)$ by simply inverting pointwise a 2D matrix.

2. Matrix Approach

The algorithm is very natural and mathematically extremely simple. Therefore, it is not surprising that it has been rediscovered independently at least three times, with some differences [1-3]. We now partly reproduce the definition and the discussion of the algorithm given in [3].

We consider a case with a purely sinusoidal forcing term S with pulsation ω. We start from the convection-diffusion equation for the generic measured quantity ξ:

---

[*] See the Appendix of F. Romanelli *et al*., Proceedings of the 23rd IAEA Fusion Energy Conference 2010, Daejeon, Korea

$$\frac{\partial \xi}{\partial t} = -\nabla \cdot \Gamma(\xi) + S, \quad \xi = \xi(r,t) \quad \Gamma = -D\nabla\xi + V\xi \tag{1}$$

After a classical integration in space, taking advantage of its linearity, we can Fourier-transform Eq. (1) in the frequency domain

$$-i\omega\xi = -\frac{1}{\mathfrak{I}'(r)}\frac{\partial}{\partial r}\left[\mathfrak{I}'(r)\left(-D\frac{\partial \xi}{\partial r} + V\xi\right)\right] + S \tag{2}$$

Where $\mathfrak{I}(r)$ is the volume enclosed inside the radial coordinate r (which can be the true physical radius or any generalized coordinate with dimension of a length); for a cylindrical system, $\mathfrak{I}(r) \propto r^2$, but generically $\mathfrak{I}$ can be a more complicated function of r. As is convenient in this kind of experiments, the signal ξ is written in terms of an amplitude and a phase: $\xi = Ae^{i\varphi}$. By integrating (2) once over the radius, and imposing the natural boundary condition $\Gamma(r=0)=0$ at the center, we obtain two real-valued algebraic equations with unknowns $(D(r),V(r))$. They take a particularly convenient expression when expressed in matrix-vector form:

$$\mathbf{M}\cdot\mathbf{Y} = \mathbf{\Gamma} \tag{3}$$

where

$$\mathbf{Y} = \begin{pmatrix} D \\ V \end{pmatrix}, \qquad \mathbf{M} = \begin{bmatrix} -A'\cos\varphi + A\varphi'\sin\varphi & A\cos\varphi \\ -A'\sin\varphi - A\varphi'\cos\varphi & A\sin\varphi \end{bmatrix},$$

$$\mathbf{\Gamma} = \begin{pmatrix} \mathfrak{I}'(r)^{-1}\int_0^r \mathfrak{I}'(z)\left(\mathrm{Re}\left(S(z)\right) - \omega A(z)\sin\varphi(z)\right)dz \\ \mathfrak{I}'(r)^{-1}\int_0^r \mathfrak{I}'(z)\left(\mathrm{Im}\left(S(z)\right) + \omega A(z)\cos\varphi(z)\right)dz \end{pmatrix}, \qquad f' \equiv \partial_r f \tag{4}$$

Let us first assume that A, φ and their first derivatives are known at radius r. Then $\mathbf{Y}$ can be straightforwardly computed by inverting the matrix $\mathbf{M}$. For this reason, in the following we refer to this method as the matrix approach.

At any point r we can compute the two eigenvalues ($\lambda_{0,1}$) and eigenvectors ($\mathbf{E}_{0,1}$) of the matrix $\mathbf{M}$: $\mathbf{M}\cdot\mathbf{E}_i = \lambda_i\mathbf{E}_i$. By writing $\mathbf{Y} = y_0\mathbf{E}_0 + y_1\mathbf{E}_1, \mathbf{\Gamma} = g_0\mathbf{E}_0 + g_1\mathbf{E}_1$, Eq. (3) becomes a couple of equations for the two unknowns $y_{0,1}$. The eigenvalues and eigenvectors depend upon the local values of (A,φ)—and their derivatives: for instance, the explicit expression for λ's is

$$\lambda = \frac{1}{2}\left[-A'\cos\varphi + A(1+\varphi')\sin\varphi \pm \sqrt{\left(A'\cos\varphi - A(1+\varphi')\sin\varphi\right)^2 - 4A^2\varphi'}\right] \tag{5}$$

A solution exists at regular points where $\mathbf{M}$ is invertible, i.e. where none of the λ's vanishes. Since $\det(\mathbf{M}) = A^2\varphi'$, singular points are where $\varphi' = 0$. The analogue of Eqns. (3,4) was first written down in [1,2] without consideration of the source term S. This is justified as long as the position of the source is detached from the volume were measurements are taken. Inclusion of the source does not alter mathematically the structure of Eqns. (3,4) but is critical empirically with regard to the appearance of singular points. Inspection of the literature shows that the fulfilment of the $\varphi' = 0$ condition coincides almost always with the location of the source (see, e.g., [4-9]). This is easily heuristically explained by noting that the l.h.s. of Eq. (2) comes as a balance between the two contributions of the r.h.s: the transport (Γ) and the source (S). If we suppose that when the source term is maximal, it dominates over the transport contribution, then we get $\xi \propto S$ and $S' = 0 \rightarrow \xi' = 0$, i.e. A'=0 and φ'=0.

At the singular points, one of the eigenvalues vanishes: $\lambda_0(r_s) = 0$. Accordingly, the l.h.s. of Eq. (3) aligns along the other eigenvector

$$\mathbf{M}\cdot\mathbf{Y} = \mathbf{M}\cdot(y_0\mathbf{E}_0 + y_1\mathbf{E}_1) = \lambda_1 y_1 \mathbf{E}_1 = \mathbf{\Gamma}, \qquad r = r_s \tag{6}$$

Physically, transport coefficients must be defined everywhere, hence Eq. (6) must admit a solution at $r = r_s$. This is possible only if its r.h.s. aligns along $\mathbf{E}_1$, too: $\mathbf{\Gamma}(r_s) = g_1\mathbf{E}_1$. Unavoidable errors present in any measurement make unlikely this case, i.e., using the data from the experiment, one expects to find points r_s where $\lambda_0(r_s) = 0$ but $\mathbf{\Gamma}(r_s) = g_0\mathbf{E}_0 + g_1\mathbf{E}_1$, with $g_0(r_s) \neq 0$. More generally, any perturbation of the values λ, $\mathbf{E}$, propagates upon $\mathbf{Y}$ as

$$\mathbf{Y} = \frac{g_0}{\lambda_0}\mathbf{E}_0 + \frac{g_1}{\lambda_1}\mathbf{E}_1 \rightarrow \delta\mathbf{Y} = \left(\frac{\delta g_0}{\lambda_0} - \frac{g_0}{\lambda_0^2}\delta\lambda_0\right)\mathbf{E}_0 + \left(\frac{\delta g_1}{\lambda_1} - \frac{g_1}{\lambda_1^2}\delta\lambda_1\right)\mathbf{E}_1 + \frac{g_0}{\lambda_0}\delta\mathbf{E}_0 + \frac{g_1}{\lambda_1}\delta\mathbf{E}_1 \tag{7}$$

Eq. (7) may be used to estimate visually how given errors on the raw data, translated into error bars for λ, $\mathbf{E}$, propagate onto $\mathbf{Y}$. It is apparent how $\delta\mathbf{Y}$ blows up when the singular points are approached:

$$\delta\mathbf{Y} \approx -\frac{g_0\delta\lambda_0}{\lambda_0^2}\mathbf{E}_0, \lambda_0 \rightarrow 0 \tag{8}$$

Even if $\mathbf{\Gamma}(r_s) \propto \mathbf{E}_1$ and Eq. (6) becomes a well-defined equation, it does not place any condition upon the full solution $\mathbf{Y}$ at $r = r_s$, but only on a subspace of it: i.e., it fixes $y_1 = g_1/\lambda_1$ whereas the component along the subspace parallel to $\mathbf{E}_0$ is undefined: any arbitrary vector aligned along the local $\mathbf{E}_0$ eigenvector can be added to the solution and still remain compatible with the data. In practice this means that only the ratio *V*/*D* can be determined at this radial location, which occurs in particular in steady-state analysis. Therefore, around singular points the MA fails but transport codes may yield deceptively accurate results: in particular the mismatch between the reconstructed values of A and φ and the experimental ones has no link at all with the error in the estimate of the values of the transport coefficients (see the discussion under Eq. (8) of [3]). Furthermore, even if the right transport profile is in the set of transport coefficient profiles provided as input to the transport code, it will be missed by the optimization procedure (see the discussion under Eq. (8) of [3]). Only at regular points transport codes can potentially attain a reconstruction of the measured value as good as that provided by the MA, provided the set of input trial profiles includes the solution given by the MA.

Experiments actually provide values for A and φ at a discrete (possibly rather coarse) set of measurement points and within some error bars. To apply the matrix method, one must first interpolate the discrete set $\{A,\varphi\}_{\text{exp}}$ with some analytical smooth curve: third order splines, e.g., are fine, since they imply continuity of the first two derivatives, in harmony with the second-order nature of eq. (1). However, this step can potentially lead to some issues, that we are going to discuss: first of all, although formally the effect of any error on $\{A,\varphi\}_{\text{exp}}$ can be propagated upon (D,V) by means of Eq. (7), this is unpractical for actual computations. A more convenient approach is statistical in nature (MonteCarlo): data are perturbed by random quantities $(A,\varphi) \rightarrow (A \pm \delta A, \varphi \pm \delta\varphi)$, where $(\delta A, \delta\varphi)$ are picked up from a statistical distribution (usually normal distribution with zero mean and standard deviation given by experimental errors). Given each such realization of the experimental data, we can interpolate them with a curve and compute accordingly the values of D and V. Repeating the whole procedure over a large number of independent runs yields a statistical distribution from which confidence intervals for the couple (D,V) can be drawn.

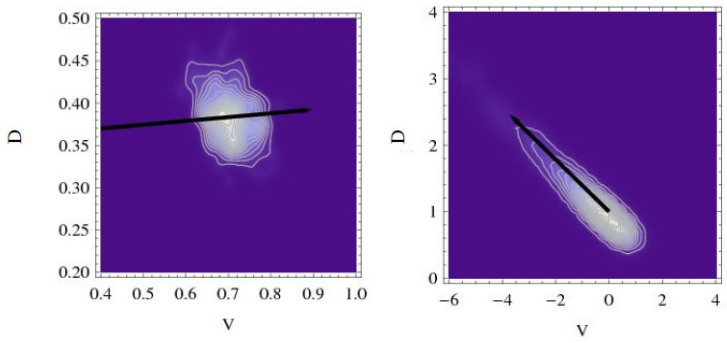

Fig. 1. Contour plot for the statistical distribution of (D,V) couples. Data are produced by 400 independent realizations of synthetic data with stochastic perturbations added. Black lines are parallel to the local $\mathbf{E}_0$ eigenvector. On the left, a regular point; on the right a singular point

A visual representation is given in Fig. (1): The clouds in the two contour plots stand for the typical distributions of the couples (D,V) that one expects after a Monte Carlo simulation taking into account errors on the data. The thick black lines are parallel to the local $\mathbf{E}_0$ eigenvector. The left plot is for a regular point: independent estimates distribute roughly as a normal distribution around the average value. The right plot shows what happens when a singular point is approached: the distribution aligns along $\mathbf{E}_0$.
This procedure has the side advantage of simultaneously accounting for some arbitrariness in the choice of the interpolating curve: for a given set of data, several different interpolating curves can be devised; this amounts to keep fixed (A, φ) in Eq. (4), but changing the derivatives (A', φ'), and can be considered as a subset of the more general Monte Carlo procedure above, where we change both the data and their derivatives. In the presence of significant errors, the random scatter between neighbouring data points, however, leads easily to the creation of spurious singular points that invalidate the analysis. In order to remove them, some manipulation of data is mandatory: either one drops the requirement of exactly interpolating the data points and replaces it with a weaker requirement, e.g., least squares fitting, or preprocesses the data by smoothing them using some filter. In both cases, the output must be a continuous function whose slope vanishes only in correspondence of the true singular points.

In conclusion, there is some arbitrariness in the choice of the set of smoothed profiles. We argue, however, that its consequence on the reconstruction is smaller than the one due to the choice of the set of transport coefficient profiles that must be provided as input to a transport code. Indeed the latter choice does not only involve a smoothing of the transport profiles, but also a guess of their values at the measurement points. Two experimentalists discussing their respective choices of the smoothing of A and φ should easily reach a consensus for a new common analysis: indeed it is just a matter of fitting measured data. Possibly the consensus analysis will provide a larger size of the uncertainty clouds with respect to their individual guesses, because of a larger flexibility of the common set of smoothed profiles. Reaching a consensus about the set of transport coefficient profiles provided as input to a transport code requires a common guess about the sought-for unknown transport profiles that may be harder to establish.

In order to clarify further the link between the reconstruction of transport codes and that of the MA, we now compare their outputs on one and the same set of data. First, we stress that $A(r)$ and $\varphi(r)$ must have smooth derivatives if the convection-diffusion equation is meant to describe the transport. Second, the MA yields exactly the values of (D ,V) provided by the code at each measurement point, if it is applied by taking the reconstructed profiles of $A(r)$ and $\varphi(r)$ produced by the code as a result of its optimization process. Indeed formulas (3) are a mere reformulation of the convection-diffusion equation, provided the flux at the origin

vanishes in the code boundary conditions, too. However the reconstructed profiles of $A(r)$ and $\varphi(r)$ do not necessarily go through the experimental error bars, while the smoothed ones used in the MA do. Third, for a given choice of a smoothed profile of $A(r)$ and $\varphi(r)$, the MA applied at all r's yields a smooth profile of (D ,V). If eq. (1) is integrated with this transport profile, then formulas (3) imply the values of A and φ provided by the integration at each measurement point will be those used as input to the MA, provided the flux at the origin vanishes in the code boundary conditions, too. If such a profile of (D ,V) is in the set of transport coefficient profiles provided as input to the transport code, the minimization process of the code will either choose this profile as an optimum, or find another one. However, in any case, the reconstructed profiles of $A(r)$ and $\varphi(r)$ will necessarily go through the experimental error bars, and will be deemed as good ones. Therefore the MA can be used to improve the inputs of transport codes. However, one may wonder why still using transport codes then, since the MA already gives good reconstructions, and with reliable error bars, what is not automatically provided by transport codes.

3. Test case simulations

In this section we show the effectiveness of the algorithm against data produced in true experiments. As a test case we refer to the shots extensively reported in the paper [9]: a set of JET L-mode-confinement discharges designed to study the transport of toroidal momentum in the presence of different torques and magnetic ripple. Global plasma parameters are: core density $\approx 3\ 10^{19}$ m^{-3}, core ion and electron temperature ≈ 3 keV, plasma current 1.5 MA, on-axis magnetic field 2.2 T and $q_{95} = 5$. Plasma is heated via NBI: 2.5 MW delivered in a continuous fashion and about 4.5 MW modulated with a 50/110 ms on/off duty cycle for experimental purposes. The resulting waveform has a dominant sinusoidal component at a frequency 6.25 Hz. The signal measured via Charge Exchange Spectroscopy is the toroidal velocity of rotation, and the corresponding source term is the torque driven by the beams. Figure (2) shows the (A,φ, S) profiles: in this case (only the fundamental harmonic is considered in this analysis), and Fig. (3) the results (D,V). The error bars were produced with the MonteCarlo procedure earlier described, over 20 independent statistical realizations. The errors on the data were chosen as: error on the amplitude = 5% of the signal, gaussian distributed; error on the phase = 11 degrees—corresponding to a time resolution of 5 ms—uniformly distributed.

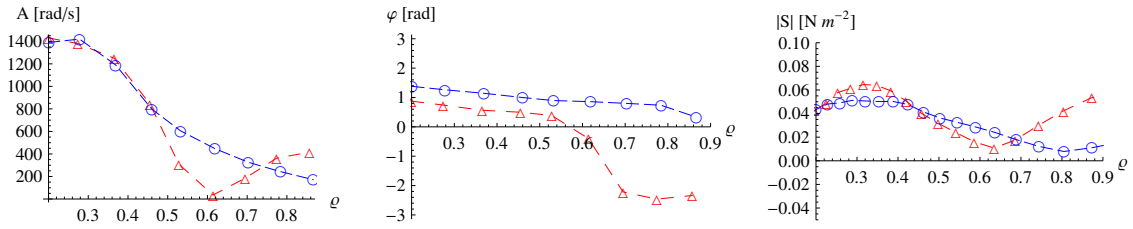

Fig. 2 Left plot, signal amplitude; center plot, signal phase; right plot, torque. The data are the same published in ref. [9] and refer to the fundamental modulation frequency ν = 6.25 Hz. Red curves with triangles refer to shot 77090; blue curves with circles, to shot 77091.

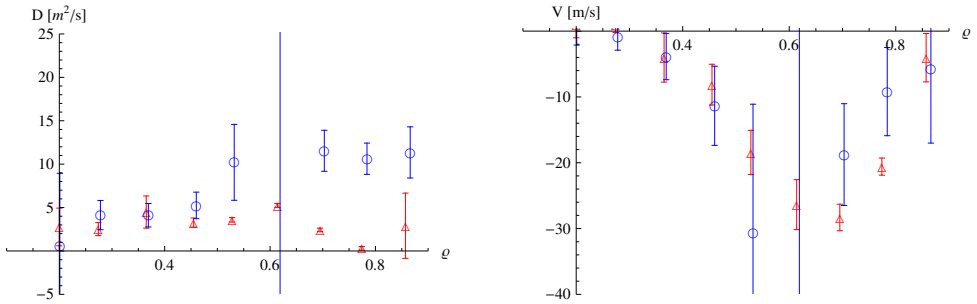

Fig. 3 Left plot, diffusivity *D*; right plot, pinch *V* for the shots 77090 (red symbols), and 77091 (blue symbols).

We point out several remarkable facts about the results displayed in Fig. (3): (i) the two discharges have compatible pinches *V*, but not diffusivities *D*, beyond about half radius. (ii) The absolute numerical values for both *D* and *V* are hardly consistent with typical JET estimates, which are usually about a factor of two smaller (see, e.g., Fig. 12(d) in [9]); (iii) the diffusivity for discharge 77090 takes suspiciously small values (practically zero or even negative) around $r = 0.8$. Such values have not physical meaning.

It is not inexplicable that two nearly identical discharges [9] do feature slightly different transport profiles, hence a mere difference between couples (*D*,*V*) is not troublesome. On the other hand, point (ii) and—above all—(iii) clearly points out to some issue with the modelling. It may be related to several different reasons, one is a bad modelling of the torque term, either due to the neglect of some contribution in the external driving, or because of the appearance of additional intrinsic torques (e.g., residual stress). A more detailed discussion of the modelling of these discharges with allowance for these additional contributions, which shows how the disagreement is eventually settled, is presented in [10]. Here, we want to stress that identification of these issues was possible because of the MA algorithm. Within the standard approach using transport codes, the two profiles *D(r)* and *V(r)* would have been taken equal a priori; accordingly the resulting discrepancy arisen in the modelled (A, φ) profiles would have been attributed generically to experimental errors (see Fig. 12 in [9]).
For comparison we present a second extensive sets of modelling, still done on JET pulses: discharges #73701-2,73704,73707-9. These are discharges explicitly designed for measuring parameteric dependence upon momentum transport and Prandtl number via NBI modulation. [11]. In Fig. (4) we show the relevant profiles of the torque and final perturbed rotation, still taken using CXRS. This time, signals are collected both at the dominant frequency (8.33 Hz) and its overtone at twice this value. The corresponding transport coefficients are computed for all available datasets and shown in Fig. (5). We recover consistent trends, although with non negligible shot-to-shot differences, which—to some extent—should be related to different plasma equilibria. In particular, the different estimates for *D* show consistent increasing trends going outward, closely resembling those of shot 77091 in Fig. (3), albeit smaller as numerical values.

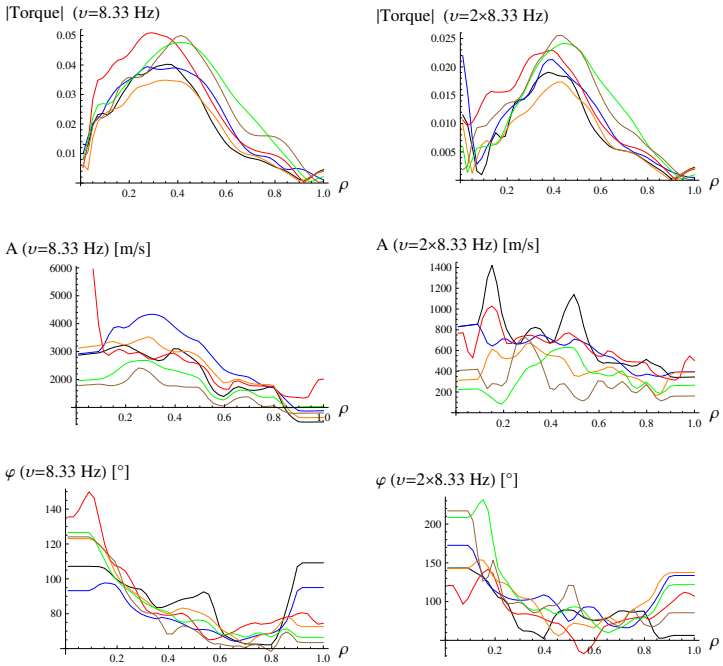

Fig. 4 From top to bottom: torque density (N m^{-2}), amplitude *A* of the perturbation, phase φ. Left column: data for the fundamental frequency of modulation.Right column: data for the first overtone. The color code is: black, shot 73701; blue, 73702; red, 73704; orange, 73707; green, 73708; brown, 73709. Here and in all the other plots, the horizontal coordinate ρ is the square root of the normalized toroidal flux

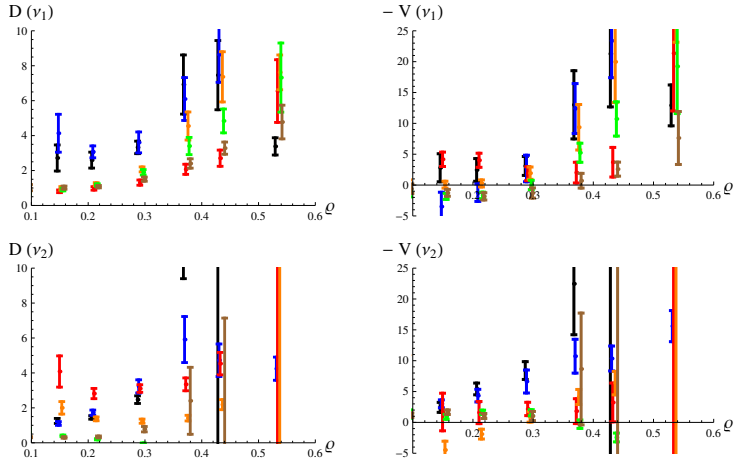

Fig. 5 Diffusivity *D* (m^2/s) and (- pinch V) (m/s) for both the fundamental frequency of modulation ν_1 and first overtone ν_2 computed from the data of Fig. (4). The color code is the same as Fig. (4). Data sets have been slightly horizontally shifted with respect to each other. The coefficients span the range $\rho < 0.55$ since in the region $0.6 < \rho < 0.8$ the phase of the signal is almost constant (fig. 4, bottom row), making the reconstruction unfeasible: this is apparent by the large error bars at the largest radii. For the same reason, some points are missing below $\rho = 0.2$.

4. Final remarks

To summarize, the MA is lighter computationally than classical transport codes. It provides a clear geometrical foundation to the nature and size of uncertainties in profile reconstruction. The reconstruction radius-by-radius enables to see how different the uncertainties over *D(r)* and *V(r)* are as a function of *r*. This uncertainty is larger in the regions where sources or sinks are present. A complete discussion of the advantages of the MA can be found in [3]. Further analysis of experimental data is in progress.

Acknowledgments
This work resulted from a long series of discussions with P. Mantica about analysis of JET data. We thank V. F. Andreev, X. Garbet and R. Paccagnella for useful remarks. This work was supported by EURATOM and carried out within the framework of the European Fusion Development Agreement. The views and opinions expressed herein do not necessarily reflect those of the European Commission

References

[1] K. Krieger, et al, Nucl. Fusion **30** (1990) 2392

[2] H. Takenaga, et al, Plasma Phys. Control. Fusion **40** (1998) 183.

[3] D.F. Escande and F. Sattin, Phys. Rev. Lett. **108** (2012) 125007.

[4] N.J. Lopes Cardozo, Plasma Phys. Control. Fusion **37** (1995) 799

[5] F. Ryter, et al, Nucl. Fusion **40** (2000) 1917

[6] P. Mantica, et al, Phys. Rev. Lett. **95** (2005)185002

[7] P. Mantica, et al, Plasma Phys. Control. Fusion **48** (2006) 385

[8] P. Mantica, et al, Fusion Sci. Technol. **53** (2008) 1152

[9] A.T. Salmi, et al, Plasma Phys. Control. Fusion **53** (2011) 085005

[10] F. Sattin, et al, invited talk at the 39th EPS Conference on Plasma Physics (Stockholm, 2012), to appear in Plasma Phys. Control. Fusion

[11] T. Tala, et al, Nucl. Fusion **51**, 123002 (2011)